Inorganic Chemistry

Article

pubs.acs.org/IC

Copper Phenanthrene Oxidative Chemical Nucleases

Zara Molphy,[†] Andreea Prisecaru,[†] Creina Slator,[†] Niall Barron,[†] Malachy McCann,[‡] John Colleran,[§] Deepak Chandran,[†] Nicholas Gathergood,[†] and Andrew Kellett*[,†]

[†]School of Chemical Sciences and National Institute for Cellular Biotechnology, Dublin City University, Glasnevin, Dublin 9, Ireland

[‡]Department of Chemistry, National University of Ireland, Maynooth, Kildare, Ireland

[§]School of Chemistry, Dublin Institute of Technology, Kevin Street, Dublin 2, Ireland

Supporting Information

ABSTRACT: Here we report the synthesis and isolation of a series of bis-chelate Cu^{2+} phenanthroline−phenazine cationic complexes of $[Cu(DPQ)(Phen)]^{2+}$, $[Cu(DPPZ)(Phen)]^{2+}$, and $[Cu(DPPN)(Phen)]^{2+}$ (where Phen = 1,10-phenanthroline, DPQ = dipyridoquinoxaline, DPPZ = dipyridophenazine, and DPPN = benzo[*i*]dipyridophenazine). These compounds have enhanced DNA recognition relative to the well-studied chemical nuclease, $[Cu(Phen)_2]^{2+}$ (bis-Phen), with calf thymus DNA binding constants of DPQ and DPPZ agents ($\sim 10^7$ $M(bp)^{-1}$) being the highest currently known for Cu^{2+} phenanthrene compounds. Complex DNA binding follows DPQ ≈ DPPZ > DPPN > bis-Phen, with fluorescence quenching and thermal melting experiments on poly[d(A-T)$_2$] and poly[d(G-C)$_2$] supporting intercalation at both the minor and major groove. Phenazine complexes, however, show enhanced targeting and oxidative cleavage on cytosine-phosphate-guanine-rich DNA and have comparable *in vitro* cytotoxicity toward the cisplatin-resistant ovarian cancer line, SKOV3, as the clinical oxidative DNA-damaging drug doxorubicin (Adriamycin). In this study we also describe how a novel "on-chip" method devised for the Bioanalyser 2100 was employed to quantify double-stranded DNA damage, with high precision, by the complex series on pUC19 DNA (49% A-T, 51% G-C). Both DPQ and bis-Phen complexes are highly efficient oxidizers of pUC19, with DPQ being the most active of the overall series. It is apparent, therefore, that oxidative chemical nuclease activity on homogeneous canonical DNA is not entirely dependent on dynamic nucleotide binding affinity or intercalation, and this observation is corroborated through catalytic interactions with the superoxide anion radical and Fenton breakdown of hydrogen peroxide.

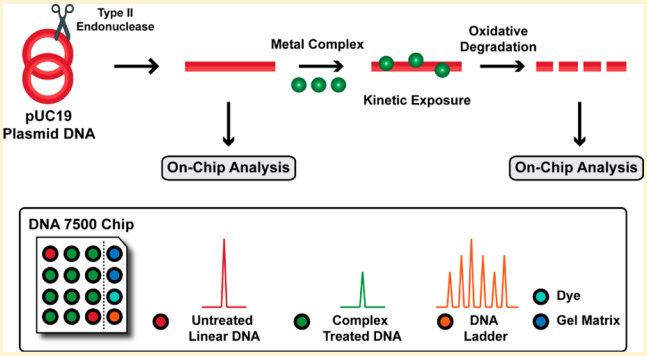

INTRODUCTION

The advent of coordinating phenanthrene-based intercalators to transition-metal cations has unveiled a new frontier for DNA-targeted metallodrug development.[1] While the application of *cis*-diamminedichloroplatinum(II) (cisplatin) continues to be a cornerstone of modern cancer chemotherapy,[2] the functionalization of this agent with intercalating ligands[3] and the construction of nonplatinum metallo-intercalators with bis- and tris-phenanthrene chelated symmetry[4] has revealed unique but structurally interrelated chemotypes of promising biological utility. Significant examples of these cationic agents (see Scheme 1) include *cis*-$[Pt(NH_3)_2(phenanthridine)Cl]^+$ (phenanthriplatin),[5] which exhibits a unique spectrum of activity within the National Cancer Institute 60-cell tumoral panel and enhanced cellular uptake relative to cisplatin; Δ-$[Ru(DPPZ)(Phen)_2]^{2+}$, which has excellent DNA recognition properties and is widely known as a "light switch" complex due to photoluminescent enhancement upon nucleotide binding;[6] and $[Cu(Phen)_2]^{2+}$, which is an effective chemical nuclease that induces DNA degradation through free-radical oxidation of deoxyribose.[7−9] Thus, by varying both the metal center and coordinated phenanthrene base, unique interactions on DNA and within human-derived cancer cells can be achieved.

The chemical nuclease $[Cu(Phen)_2]^{2+}$ is capable of abstracting hydrogen ($^{\bullet}H$) from the pentose ring of DNA in the presence of both exogenous reductant ($Cu^{2+} \rightarrow Cu^+$) and oxidant (O_2 or H_2O_2), under a quasi-reversible electrochemical process,[7,8] and has served as an important template for cytotoxic metallodrug design.[10] The mechanism of abstraction is sequential and is dependent on both Cu^+ and hydrogen peroxide (H_2O_2).[11] Furthermore, the production of H_2O_2 in the reaction is believed to result from superoxide dismutase (SOD) mimetic activity,[12] post electron-transfer from Cu^+ to O_2. $[Cu(Phen)_2]^{2+}$ oxidizes DNA without specificity, predominately at the minor groove, and in an effort to improve this lack of specificity, chimeric $[Cu(Phen)_2]^{2+}$ molecules have been generated using target-specific, DNA-recognition vectors of single-stranded DNA[13,14] and also with the adenine−thymine (A-T) specific minor-groove binder distamycin.[15,16]

Received: April 22, 2014
Published: May 7, 2014

   dx.doi.org/10.1021/ic500914j | *Inorg. Chem.* 2014, 53, 5392−5404

Scheme 1. Molecular Structures of Cytotoxic Platinum(II) Complexes Cisplatin and Phenanthriplatin, the Ruthenium(II) DNA Light Switch Complex Δ-$[Ru(DPPZ)(Phen)_2]^{2+}$, and the Copper(II) Chemical Nuclease $[Cu(Phen)_2]^{2+}$

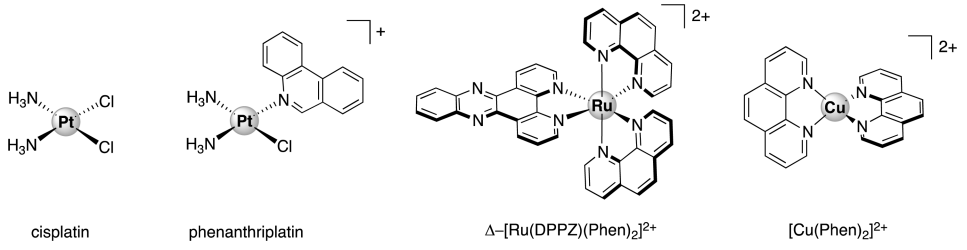

Scheme 2. Molecular Structures of the Cu^{2+} Coordination Complexes 1−4

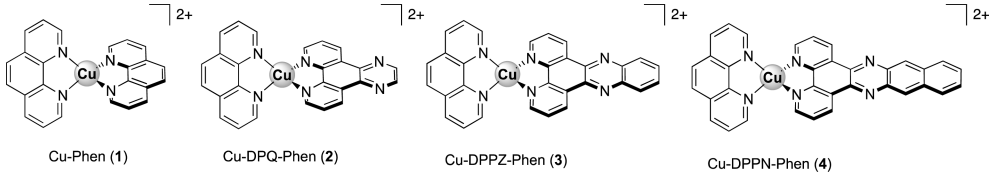

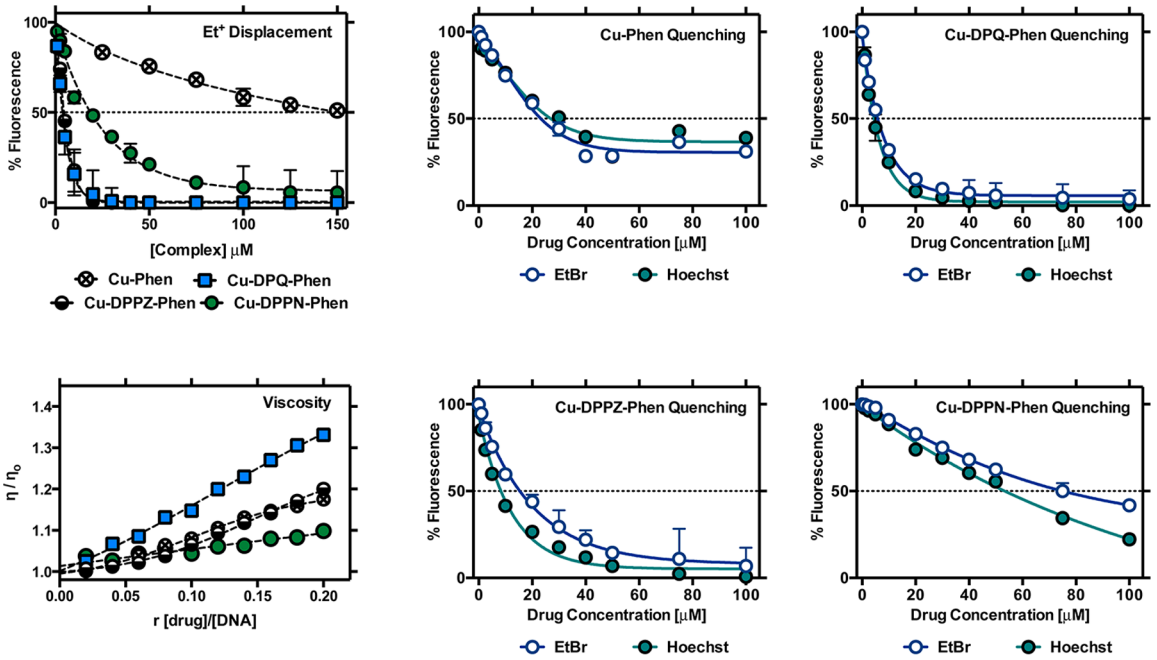

Figure 1. Binding of Cu^{2+} complexes **1−4** to ethidium-saturated solutions of dsDNA (ctDNA), fluorescence quenching of limited ethidium bromide or Hoechst 33258 bound dsDNA (ctDNA) upon titration of complex, and viscosity properties of complex treated salmon testes dsDNA. (Data points presented as an average of triplicate fluorescence measurement ± standard deviation (S.D.))

In this study we report the synthesis and isolation of a series of bis-chelate Cu^{2+} phenanthroline−phenazine cationic complexes of $[Cu(DPQ)(Phen)]^{2+}$, $[Cu(DPPZ)(Phen)]^{2+}$, and $[Cu(DPPN)(Phen)]^{2+}$ (where DPQ = dipyrido[3,2-*f*:2′,3′-*h*]quinoxaline, DPPZ = dipyrido[3,2-*a*:2′,3′-*c*]phenazine, and DPPN = benzo[*i*]dipyrido[3,2-*a*:2′,3′-*c*]phenazine) (Scheme 2). Since designer metal-chelating phenazine ligands have shown interesting potential within Ru^{2+} DNA-selective binding probes,[17−20] a question remains unanswered regarding their application within Cu^{2+} complexes toward (i) nucleotide equilibrium binding affinity, base-specific targeting and intercalation, (ii) oxidative chemical nuclease activity, (iii) redox behavior including interactions with superoxide and hydrogen peroxide, and (iv) cytotoxicity toward platinum-resistant human-derived cancer cells. Our aim here was to investigate how systematic extension of the ligated phenazine ligand influences DNA recognition and oxidative degradation, and how this study can ultimately supply basic information toward the design of enhanced artificial chemical nucleases of biological utility. To identify and compare the DNA degradation profiles in this family of structurally related compounds, we proposed the development of a capillary electrophoresis microfluidic chip assay for the Bioanalyzer 2100 (Agilent Technologies), which is capable of high-resolution sizing and quantitation of dsDNA (ds = double-stranded) fragments based on normalization to internal markers and a standard DNA ladder.[21−23]

RESULTS

Preparation of the Complexes. The quinoxaline and phenazine ligands (DPQ, DPPZ, and DPPN) were generated

dx.doi.org/10.1021/ic500914j | Inorg. Chem. 2014, 53, 5392−5404

Table 1. DNA Binding Properties

compound	C_{50}[a]	K_{app} M(bp)$^{-1}$[b]	Q Hoechst[c]	Q ethidium[c]	η/η_o[d]
netropsin	46.27	2.50×10^6	02.40	20.04	1.00
Actinomycin D	04.10	2.92×10^7	26.34	04.78	1.14
$[Co(NH_3)_6]Cl_3$	>300		23.18	273.62	0.82
Cu-Phen[28]	179.21	6.67×10^5	34.96	20.38	1.17
Cu-DPQ-Phen	03.93	3.04×10^7	04.33	06.10	1.33
Cu-DPPZ-Phen	04.63	2.58×10^7	07.69	16.12	1.20
Cu-DPPN-Phen	18.72	6.40×10^6	56.57	75.10	1.10

[a] C_{50} = concentration required to reduce fluorescence by 50%. [b] $K_{app} = K_e \times 12.6/C_{50}$ where $K_e = 9.5 \times 10^6$ M(bp)$^{-1}$. [c] Reduction of 50% initial fluorescence from DNA-bound dye by tested compound (μM). [d] Relative viscosity value at $r = 0.20$.

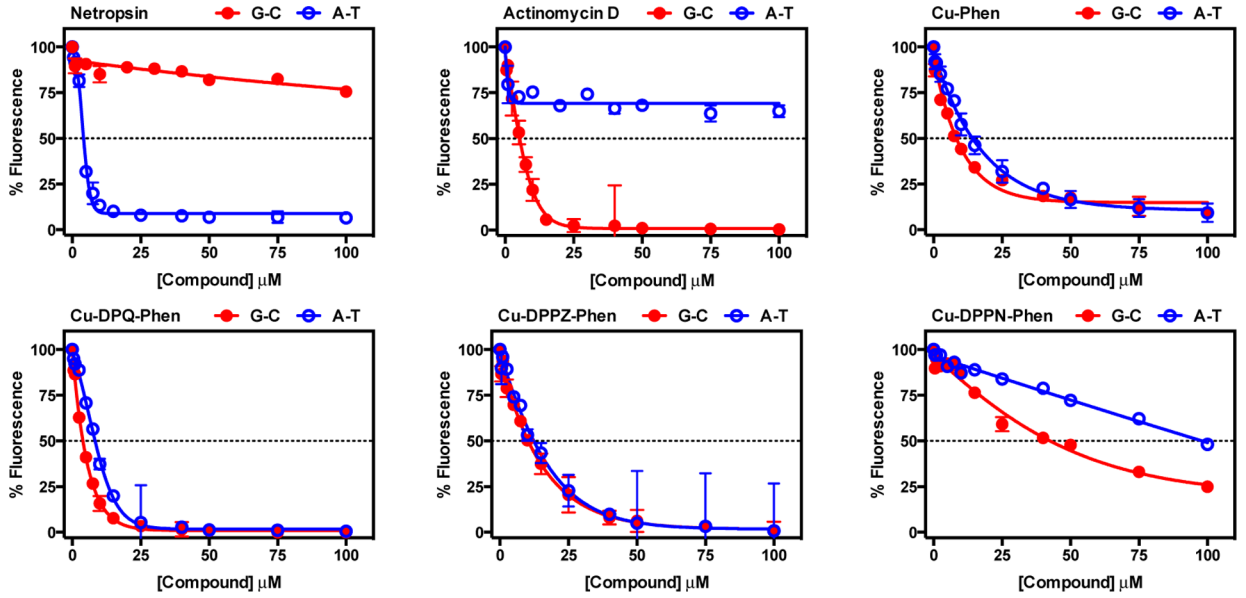

Figure 2. Fluorescence quenching of limited bound intercalator (ethidium bromide) to poly[d(G-C)$_2$] and poly[d(A-T)$_2$] upon titration of netropsin, Actinomycin D, and Cu^{2+} complexes. (Data points presented as an average of duplicate fluorescence measurement ± S.D.)

through Schiff-base condensation reactions of 1,10-phenanthroline-5,6-dione with either ethylenediamine, *o*-phenylenediamine, or 2,3-diaminonaphthalene, with some modification to previously reported methods.[24−26] The bis-phenanthroline complex $[Cu(Phen)_2](NO_3)_2$ (**Cu-Phen**, **1**) was prepared by aqueous−ethanol reflux of 1,10-phenathroline with copper(II) nitrate (2:1).[27] The complexes $[Cu(DPQ)(Phen)](NO_3)_2$ (**Cu-DPQ-Phen**, **2**), $[Cu(DPPZ)(Phen)](NO_3)_2$ (**Cu-DPPZ-Phen**, **3**), and $[Cu(DPPN)(Phen)](NO_3)_2$ (**Cu-DPPN-Phen**, **4**) (Scheme 2) were generated by first isolating the mono-phenanthroline complex $[Cu(Phen)](NO_3)_2$ and subsequently treating this with 1 equiv of the corresponding phenazine ligand.

Binding Affinity to Calf Thymus and Salmon Testes DNA. The DNA binding affinity of the complex series was determined using calf-thymus DNA (ctDNA, Ultra-Pure, Invitrogen) and salmon testes dsDNA (Sigma) by ethidium bromide and Hoechst 33258 fluorescence quenching and competition studies[28] and also through viscosity analysis (Figure 1 and Table 1). The presence of phenazine ligands in the complex cation function to significantly enhance ctDNA binding affinity with K_{app} (apparent DNA binding constant) values for **Cu-DPQ-Phen** and **Cu-DPPZ-Phen** reagents being at the order of $\sim 3 \times 10^7$ M(bp)$^{-1}$ and of similar magnitude as the intercalating polypeptide antibiotic, Actinomycin D. The DPPN-containing complex, although binding by an order of magnitude over **Cu-Phen**, was the lowest ctDNA-binding phenazine complex, at $\sim 6 \times 10^6$ M(bp)$^{-1}$. Fluorescence quenching (*Q*) of limited bound Hoechst 33258 (minor-groove binder) and ethidium bromide (intercalator) bound ctDNA were examined to identify potential binding specificity. Unlike the classical intercalator Actinomycin D and minor-groove binding agent netropsin, the complex series did not display a large degree of discrimination for quenching either of the selected fluorophores. The quenching effects of the DPQ and DPPZ complexes are stronger, overall, than **Cu-Phen**; however, this trend is reversed as the phenazine agents displace bound Hoechst with slightly more efficiency than ethidium bromide compared with **Cu-Phen**. Viscosity analysis on salmon testes dsDNA fibers revealed **Cu-DPQ-Phen** as having a significant intercalating (hydrodynamic) binding effect, followed thereafter by **Cu-DPPZ-Phen**, **Cu-Phen**, and finally **Cu-DPPN-Phen**. In nearly all experiments conducted, the Cu^{2+} complexes exhibited distinctive behavior compared to the simple $[Co(NH_3)_6]^{3+}$ complex, which is known only to have electrostatic binding affinity to the surface of DNA. Indeed this effect was confirmed by our analysis of its inability to displace intercalated ethidium, enhanced ability to displace minor-groove, surface-bound Hoechst 33258, and an overall decrease in relative viscosity.

Binding Affinity to Double-Stranded Synthetic Co-polymers of Adenine−Thymine (A-T) and Guanine−Cytosine (G-C). To explore base-specific nucleotide binding by

dx.doi.org/10.1021/ic500914j | Inorg. Chem. 2014, 53, 5392−5404

this series, synthetic alternating copolymers of adenine–thymine, poly[d(A-T)$_2$], and guanine–cytosine, poly[d(G-C)$_2$], were examined through fluorescence quenching and thermal melting analysis. Fluorescence quenching was conducted by first introducing a limited concentration (5 μM) of ethidium bromide with synthetic polynucleotide (25 μM). The complex series, along with the classical intercalator Actinomycin D and minor-groove binder netropsin, was also examined across the concentration range of 1–200 μM (Figure 2 and Table 2). The standard agents, as predicted, were highly

Table 2. Fluorescence Quenching (Q) of Limited Ethidium Bromide (5 μM) Bound Poly[d(G-C)$_2$] and Poly[d(A-T)$_2$] (25 μM) by Standard Agents Netropsin, Actinomycin D, and Cu^{2+} Complexes

compound	Q (μM) poly[d(A-T)$_2$]	Q (μM) poly[d(G-C)$_2$]
netropsin	4.08	≫200
Actinomycin D	≫200	5.47
Cu-Phen	13.34	7.96
Cu-DPQ-Phen	8.34	3.97
Cu-DPPZ-Phen	11.60	10.12
Cu-DPPN-Phen	96.56	44.18

specific in their quenching of either poly[d(A-T)$_2$] (netropsin) or poly[d(G-C)$_2$] (Actinomycin D). A-T-rich polymers are known to have "T-tract structure", which features a compressed minor groove and a shorter helical repeat of 10 bp per turn, compared to 10.5 bp per turn determined for canonical B-DNA. As such, these polymers are excellent substrates for minor-groove binding drugs, and this interaction was evident in these experiments with netropsin. G-C-rich polymers, conversely, can have up to 12 bp per helical turn and are known to form left-handed "Z-DNA" conformations with a helical rise per base pair dimer of ∼7.4 Å. These polymers, therefore, are highly suited for intercalative binding by agents such as Actinomycin D. It was also evident that both netropsin and Actinomycin D were selective in their binding interactions and thus did not quench fluorescence (up to 200 μM) on disfavored DNA polymers of poly[d(G-C)$_2$] and poly[d(A-T)$_2$], respectively. The Cu^{2+} complexes displayed effective quenching on both A-T and G-C polymers and so could not be characterized by either classical binding mode alone. Each complex was found to have a slight preference for ethidium quenching on poly[d(G-C)$_2$], with **Cu-DPQ-Phen** displaying the highest overall activity in the series, followed thereafter by **Cu-DPPZ-Phen**, **Cu-Phen**, and finally **Cu-DPPN-Phen**.

Thermal melting studies were also conducted on poly[d(G-C)$_2$] and poly[d(A-T)$_2$] synthetic nucleotides exposed to the complex series, netropsin, and Actinomycin D (Table 3) (see Supporting Information for optimization studies). Thermal melting (T_M) marks the midpoint in the melting process of DNA when a 50:50 equilibrium exists between the helical and single-stranded state. This method of analysis offers a useful insight into the strength of interaction between a drug and nucleic acid; the stronger this interaction, the more energy required to denature the stabilized secondary structure relative to the untreated polynucleotide (ΔT_M). As expected, Actinomycin D substantially stabilized the thermal denaturation of poly[d(G-C)$_2$] (ΔT_M + 12.10 ± 0.95 °C). Similarly, the minor-groove binding drug netropsin gave an almost equal magnitude of stabilization on the thermal melting of poly[d(A-T)$_2$] (ΔT_M + 12.32 ± 0.79 °C). Further, these classical agents had either low or no stabilization effects on disfavored nucleotide polymers, again highlighting their nucleotide binding specificity. The Cu^{2+} complexes all stabilized the thermal melting temperature of poly[d(G-C)$_2$] to varying extents and more closely demonstrated thermochemical behavior in line with intercalator Actinomycin D. **Cu-DPQ-Phen** had the strongest stabilizing effect (ΔT_M + 11.39 ± 1.10 °C) on G-C, and this was followed closely by the **Cu-DPPZ-Phen** complex (ΔT_M + 10.44 ± 1.10 °C). To a lesser extent, **Cu-Phen** also enhanced the melting temperature of G-C (ΔT_M + 6.64 ± 1.58 °C), while the DPPN agent was only weakly stabilizing (ΔT_M + 2.10 ± 1.03 °C). In contrast to G-C polynucleotides, all complexes had negligible or negative effects on the thermal stabilization of poly[d(A-T)$_2$], thus reflecting similarity with Actinomycin D in this regard.

Chemical Nuclease Activity. The oxidative chemical nuclease activity of the complex series was identified using a novel "on-chip" method devised for the Agilent 2100 Bioanalyzer, which is outlined in Figure 3. The DNA 7500

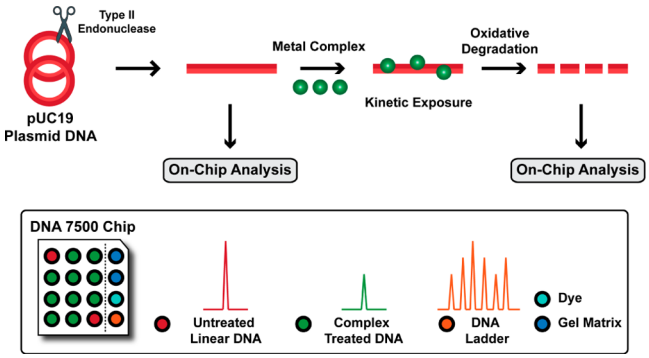

Figure 3. "On-Chip" protocol for examining artificial metallonuclease activity using the Bioanalyzer 2100.

microfluidic chip was employed as it can detect and quantify linear dsDNA fragments sized between 100 and 7500 bp by

Table 3. Influence of Standard Agents (Netropsin, Actinomycin D) and Copper Phenazine Complexes on the Thermal Denaturation of Poly[d(G-C)$_2$] and Poly[d(A-T)$_2$] Alternating Copolymers

compound	ΔT_M[a] (°C) poly[d(A-T)$_2$]	ΔT_M[a] (°C) poly[d(G-C)$_2$]
netropsin	12.32 ± 0.79	2.83 ± 0.38
Actinomycin D	−0.32 ± 0.29	12.10 ± 0.95
Cu-Phen	−0.02 ± 0.29	6.64 ± 1.58
Cu-DPQ-Phen	0.60 ± 0.18	11.39 ± 1.10
Cu-DPPZ-Phen	0.50 ± 0.10	10.44 ± 1.10
Cu-DPPN-Phen	−0.39 ± 0.21	2.10 ± 1.03

[a] ΔT_M = difference in thermal melting (T_M) of drug-treated nucleotide at r = 0.1 compared with drug-untreated nucleotide.

dx.doi.org/10.1021/ic500914j | Inorg. Chem. 2014, 53, 5392–5404

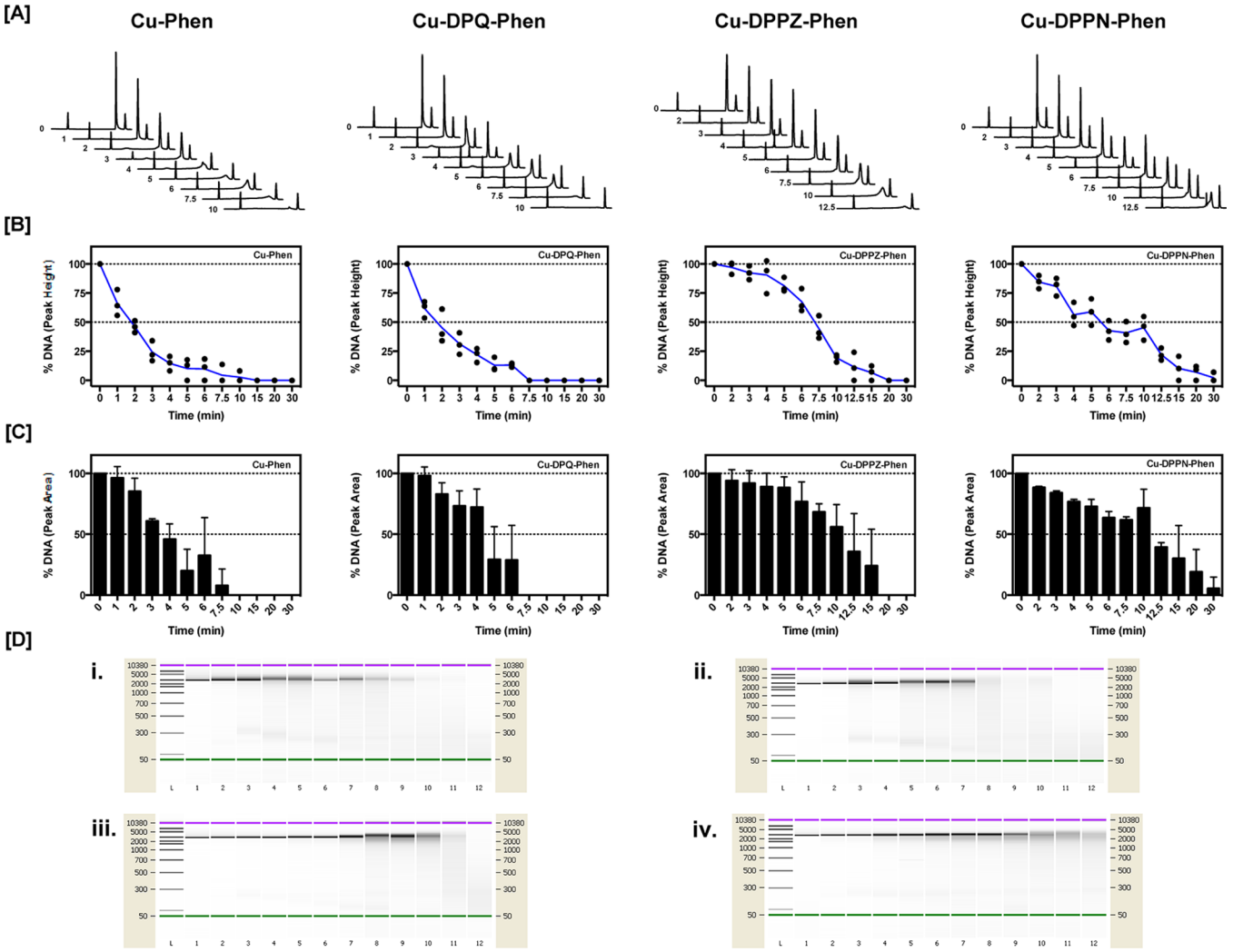

Figure 4. (A) Electrograms of linearized pUC19 (400 ng) exposed to metal complex (500 nM) between 0 and 12.5 min on the Bioanalyzer 2100 with DNA 7500 microfluidic chips, (B) %DNA degradation (from peak height analysis of triplicate experiments) of pUC19 exposed to Cu^{2+} complexes between 0 and 30 min, (C) %DNA degradation (from peak area analysis of triplicate experiments, error bars ± S.D.) of pUC19 exposed to Cu^{2+} complexes between 0 and 30 min, and (D) typical electropherograms generated by the Bioanalyzer 2100, L = ladder, lane 1 = pUC19 control, lanes 2−12 = pUC19 + complex exposed between 1 and 15 min for bis-Phen (i) and DPQ-Phen (ii) samples, and between 1 and 30 min for DPPZ-Phen (iii) and DPPN-Phen (iv) samples.

capillary electrophoresis. Superhelical plasmid DNA (pUC19, 2686 bp) was generated by *Escherichia coli* and subsequently linearized by the type II endonuclease *Hin*dIII, which has one recognition sequence on this vector. Linear pUC19 (400 ng) was then purified on an anion-exchange column (Qiagen) and incubated with 500 nM of complex, under standard atmospheric conditions, in the presence of 1 mM reductant (sodium L-ascorbate). At successive time periods, between 1 and 30 min, aliquots were removed from each reaction and quenched with 100 μM of both 2,9-dimethyl-1,10-phenanthroline (neocuproine) and ethylenediaminetetraacetic acid (EDTA). Complex-treated and untreated linear DNA samples (1 μL) were then loaded onto the Agilent DNA 7500 microfluidic chip. Further, sample wells were also loaded with standard DNA markers sized at 50 and 10 380 bp, which are evident in each electrogram. Untreated pUC19 produced a single high-resolution peak located at ~2870 bp (Figure 4A, time = 0), which was within the experimental error margin for nucleotide sizing accuracy (±10% coefficient of variation). Degradation of pUC19 by each complex was followed by a reduction in peak area and peak height intensity and was accompanied by asymmetric tailing, which is indicative of smaller fragments being sheared off through chemical nuclease activity. Typical electrograms generated are shown in Figure 4A, which details the untreated control DNA (time = 0) and each copper complex kinetically exposed to pUC19 at specific time points indicated. Further, typical electropherograms generated by each complex are shown in Figure 4D, which details the standard DNA ladder (L), untreated control pUC19 (lane 1), and complex-treated DNA between either 1−15 min (for **Cu-Phen** and **Cu-DPQ-Phen** complexes) or 1−30 min (for **Cu-DPPZ-Phen** and **Cu-DPPN-Phen** complexes) (lanes 2−12). In our preliminary experiments we discovered that bis-phen and DPQ complexes were much more efficient in degrading pUC19; hence, our analysis on the Bioanalyzer was conducted on a shorter time frame for both these agents. Quantification of pUC19 damage was achieved (Figure 4, center) using peak height reduction and peak area reduction analysis from triplicate electrograms, and comparisons of cleavage efficiency were made based on the time taken to

dx.doi.org/10.1021/ic500914j | *Inorg. Chem.* 2014, 53, 5392−5404

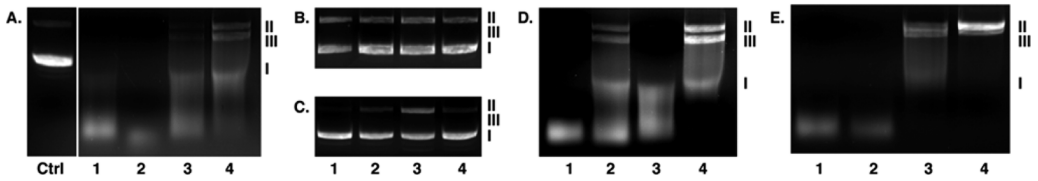

Figure 5. Agarose gel electrophoresis of purified (EDTA-free) supercoiled pUC19 (400 ng) with 1 mM Na-L-ascorbate incubated for 30 min with 500 nM metal complexes (A), and in the presence of 1000 units of bovine liver catalase (B), 100 μM neocuproine (C), 1000 units of bovine SOD (D), and 10% v/v DMSO (E). Ctrl = pUC19 complex-untreated control, lanes 1−4 = 500 nM **Cu-Phen**, **Cu-DPQ-Phen**, **Cu-DPPZ-Phen**, and **Cu-DPPN-Phen**, respectively.

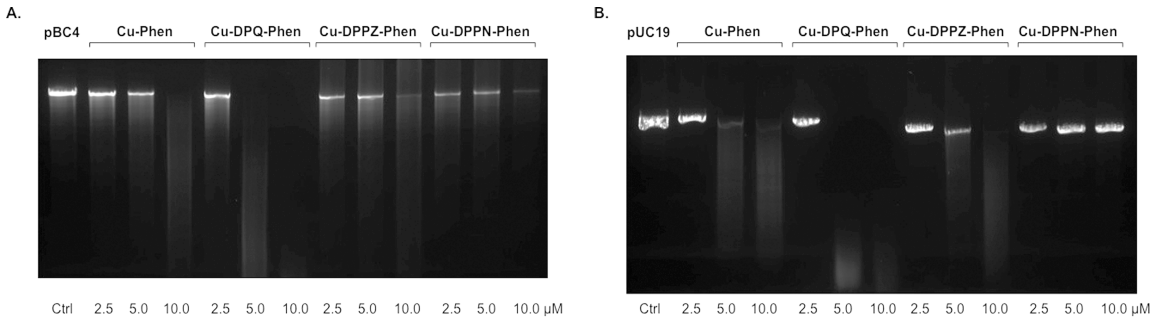

Figure 6. Degradation of 400 ng of linearized plasmid pBC4 (A) and pUC19 (B) DNA with tested metal complex (2.5, 5.0, and 10.0 μM) in the presence of added reductant (1 mM) for 30 min at 37 °C; (A) pBC4 (59% G-C); (B) pUC19 (51% G-C).

degrade 50% (D_{50}) of pUC19, with 100% being taken as the normalized intensity of triplicate-untreated pUC19 DNA. Both **Cu-Phen** and **Cu-DPQ-Phen** are remarkably efficient in degrading dsDNA and are similar, in terms of both their D_{50} values and overall profile. Analysis by pUC19 peak height reduction shows that both agents similarly reduce intensity, by 50%, after ∼2 min; however, **Cu-Phen** has a marked enhancement over **DPQ-Phen** between 4.0 and 7.5 min on comparison of peak area degradation. Nonetheless, the DPQ agent totally degrades the plasmid by 7.5 min under both analyses, whereas it is ∼10 min before this is achieved by **Cu-Phen**. The DPPZ and DPPN reagents are less efficient in their chemical nuclease activity, with **Cu-DPPZ-Phen** displaying rapid degradation between 5 and 12.5 min ($D_{50} \approx 7.5$ min by peak height), while **Cu-DPPN-Phen** delivers a somewhat linear profile over the complete time frame ($D_{50} \approx 12.5$ min by peak height). Further evidence the DPPZ agent is a more efficient chemical nuclease compared with **Cu-DPPN-Phen** can be gleaned from peak area analysis. DPPZ completely digests the plasmid by ∼20 min, while at the end of our analysis (30 min) a small concentration of nucleotide remained within the DPPN-treated sample.

Interactions with Superhelical pUC19. The interaction of purified superhelical pUC19 (generated using *E. coli* as described above) with the complex series was studied under similar conditions (500 nM [complex] with 1 mM reductant) (Figure 5) using standard agarose gel electrophoresis. All complexes induced complete degradation of the superhelix with the exception of **Cu-DPPN-Phen**, where evidence of nicked (Form I) and linear (Form II) tertiary conformations remained after 30 min. The importance of Cu^+ and hydrogen peroxide in the cleavage mechanism was demonstrated by the complete inhibition of nuclease activity upon addition of 1000 U of bovine liver catalase (Figure 5B) and 100 μM neocuproine (Figure 5C). Further trapping studies revealed that bovine superoxide dismutase (1000 U, Figure 5D) could strongly inhibit **Cu-DPPN-Phen** from plasmid digestion, and this complex, along with **Cu-DPPZ-Phen**, was also impeded by the hydroxyl radical scavenger dimethyl sulfoxide (DMSO) (10% v/v, Figure 5E).

Comparison Study of pUC19 and pBC4 Cleavage Efficacy. To determine the chemical nuclease on DNA of different guanine−cytosine (G-C) compositions, commercially available pUC19 (2686 bp, 51% G-C, NEB, N3033L), and pBC4 (10673 bp, 59% G-C, donated by NEB) were analyzed using gel electrophoresis in the presence of 1 mM solution of added reductant (Na-L-ascorbate). Note that both plasmids are supplied in EDTA-buffered solution, and, thus, chemical nuclease activity was examined at higher complex concentration. Further, the pBC4 plasmid was amplified in a *recA+ E. coli* host and so does not have dimer deficiency usually associated with commercially available strains used for plasmid production. As a consequence, pBC4 migrates as two bands: the plasmid monomer followed by the dimer, and so this plasmid is not suitable to identify conversion among superhelical (Form I), nicked (Form II), or linear (Form III) conformations due to the overlapping nature of the dimer and Form II or Form III bands. This plasmid, however, can be exploited for artificial metallonuclease activity in its linearized form, and we employed the type II endonuclease *Age*I to generate Form III of the plasmid. For comparison purposes, pUC19 was also required in a linearized form, and this was completed using the type II endonuclease *Sca*I. Both pBC4 and pUC19 (400 ng) were then exposed, over 30 min, to between 2.5 and 10.0 μM solution of the complex series, in the presence of 1 mM exogenous ascorbate, with each reaction containing the same amount of EDTA (40.0 μM) (Figure 6). The chemical nuclease activity of **Cu-DPQ-Phen** and **Cu-DPPZ-Phen** were found to be independent of %G-C content, with the DPQ complex being the most effective cleaving agent, overall, inducing complete digestion of both pUC19 and pBC4 upon 5 μM exposure. **Cu-DPPN-Phen** was found to have a remarkably low effect on pUC19 oxidation but was more reactive toward pBC4. In contrast to the observed activities of the phenazine

dx.doi.org/10.1021/ic500914j | *Inorg. Chem.* 2014, 53, 5392−5404

reagents, **Cu-Phen** was selectively reactive toward the plasmid of lower %G-C content, and this was evidenced through complete disappearance of pUC19 at a 5 μM, while the majority of pBC4 remained unaffected under identical conditions.

The final aspect of this study involved the characterization of nuclease activity on commercial (EDTA buffered) supercoiled pUC19 plasmid. In this experiment a fixed concentration of metal complex (10 μM) was exposed to 400 ng of superhelical DNA over 30 min in the presence of 1 mM added reductant (Figure 7), and reactions all contained a final EDTA concentration of 56 μM. Surprisingly, **Cu-Phen** was found to only partially nick (Form I → Form II) pUC19, while **Cu-DPPN-Phen** had little or no oxidative affect. **Cu-DPQ-Phen** and **Cu-DPPZ-Phen**, however, facilitated complete conversion to the nicked form (Form II) of pUC19, and this observation supports the enhanced stability of these chemical nucleases within a competing, EDTA-chelated, environment.

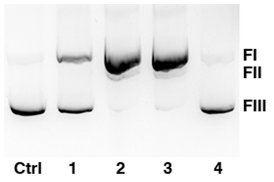

Figure 7. DNA cleavage reactions with 10 μM of **Cu-Phen**, **Cu-DPQ-Phen**, **Cu-DPPZ-Phen**, and **Cu-DPPN-Phen** (lanes 1−4, respectively) with 400 ng of commercial (EDTA buffered) superhelical pUC19. Reactions were carried out with added Na-L-ascorbate (1 mM) over 30 min at 37 °C.

***In vitro* Cytotoxicity toward SKOV3 Cancer Cells.** Flow cytometric analysis using Guava ViaCount reagent was used to examine the cytotoxic properties of the complex series and the clinical antitumor agent doxorubicin on human SKOV3 ovarian cancer cells. This cell line was selected as it possesses both a mutant *p53* gene and is intrinsically resistant to cisplatin.[29,30] The ViaCount reagent determines viability of a cell population based upon differential membrane permeability of two fluorescent DNA intercalators that classify live and dead cell ratios. SKOV3 cells were incubated with drug concentrations ranging from 100 to 0.10 μM over 24 h (Figure 8). Cytotoxicity data used to calculate the IC_{50} values (at the 95% confidence interval) were derived from sigmoidal, nonlinear regression curves (Supporting Information, Figure S5). The IC_{50} complex trend follows **Cu-DPPZ-Phen** > **Cu-DPQ-Phen** > **Cu-Phen** > **Cu-DPPN-Phen**, with all compounds exhibiting significant 24 h *in vitro* cytotoxicity values of 0.59, 1.34, 1.40, and 3.55 μM, respectively. The most active complex, **Cu-DPPZ-Phen**, is comparable to that of the clinically used chemotherapeutic drug doxorubicin, with both agents exhibiting potent inhibitory values in the nanomolar region. Indeed, doxorubicin (Adriamycin) was specifically selected for this study due to its clinical DNA-damaging properties related to intercalation and topoisomerase II inhibition.[31−33]

Electrochemistry and Redox Interactions with the Superoxide Radical Anion and Hydrogen Peroxide. The electrochemical behavior of each complex was investigated in the absence and presence of an excess of Na-L-ascorbate and hydrogen peroxide (Figure 9). All complexes exhibit well-defined, quasi-reversible redox profiles, with added oxidant or reductant having little effect on the reversibility of electron-transfer reactions for each complex. Added reductant does shift the redox potentials anodically, while added oxidant shifts the complex redox potentials to more cathodic values. Interestingly, added reductant does increase the concentration of Cu(I) species in solution; this is reflected in the observed enhancement of complex oxidation peak currents. Conversely, on addition of peroxide, the expected increase in reduction peak currents for each complex, corresponding to a solution-phase increase in Cu(II) species, is not observed. Thus, a kinetic constraint exists in the electrochemical regeneration of Cu(I) in the presence of oxidant and may be indicative of the presence of copper-hydroperoxo species being generated in solution. The superoxide dismutase mimetic (SODm) properties of the group were investigated using the nitro blue tetrazolium (NBT) assay, where a xanthine/xanthine oxidase system served as the source of superoxide radical anion ($O_2^{\bullet-}$).[34] All complexes displayed similar, concentration-dependent, SODm activity (Figure 10b) and have notable catalytic rates with K_{cat} values ranging between 9.80×10^6 M^{-1} s^{-1} (**Cu-DPPZ-Phen**) and 7.64×10^6 M^{-1} s^{-1} (**Cu-DPPN-Phen**). Complexes were then examined for their Fenton-like activity using the Amplex Red hydrogen peroxide assay (Invitrogen). None of the compounds were found to degrade H_2O_2 (5 μM) in the absence of reductant (results not shown); however, in the presence of Na-L-ascorbate (100 μM) all four chemical nucleases displayed one-phase exponential decay of peroxide (Figure 10a and Table 4). The rate of degradation, overall, is kinetically sluggish, with the rate constants for **Cu-Phen** and **Cu-DPQ-Phen** being 3.22 and 3.54 s^{-1}, respectively, and being more than twice that of **Cu-DPPZ-Phen** (1.56 s^{-1}) and **Cu-DPPN-Phen** (1.26 s^{-1}) complexes. Significantly, there was overlap between Fenton behavior and chemical nuclease activity with the most efficient

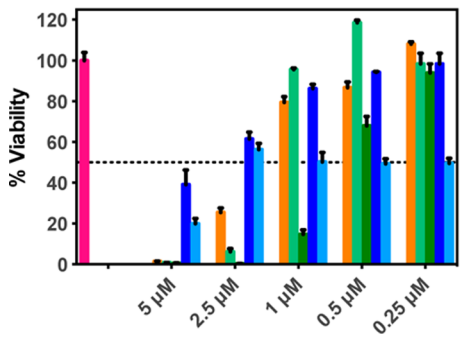

Compound	IC_{50} (μM)
Cu-Phen	1.40
Cu-DPQ-Phen	1.34
Cu-DPPZ-Phen	0.59
Cu-DPPN-Phen	3.55
Doxorubicin	0.52

Figure 8. Dose-response inhibition and IC_{50} values (at the 95% confidence interval) of Cu^{2+} complexes and the clinical agent, doxorubicin, within SKOV3 human cancer cells over 24 h of drug exposure.

dx.doi.org/10.1021/ic500914j | *Inorg. Chem.* 2014, 53, 5392−5404

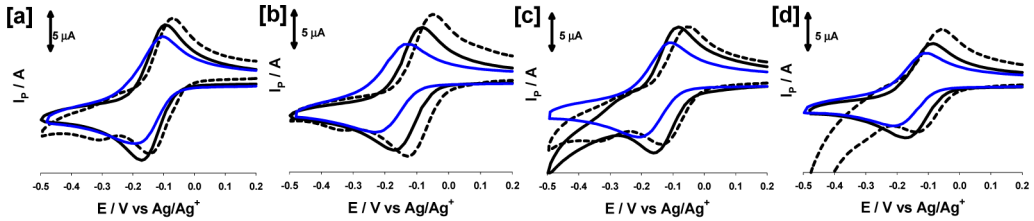

		[i]			[ii]			[iii]		
Entry	Complex	E_{Pa}	E_{Pc}	ΔE_P	E_{Pa}	E_{Pc}	E_{Pa}	E_{Pa}	E_{Pc}	ΔE_P
[a]	1	-0.096	-0.171	0.075	-0.074	-0.137	0.069	-0.104	-0.190	0.086
[b]	2	-0.081	-0.175	0.094	-0.051	-0.129	0.078	-0.124	-0.211	0.087
[c]	3	-0.082	-0.162	0.080	-0.057	-0.131	0.074	-0.105	-0.211	0.106
[d]	4	-0.100	-0.181	0.081	-0.060	-0.144	0.084	-0.100	-0.190	0.090

Figure 9. Cyclic voltammograms describing the redox behavior of 1 mM of complex, at a scan rate of 100 mV s^{-1} (solid black trace) and in the presence of 2 mM Na-L-ascorbate (dashed black trace), 2 mM H_2O_2 (solid blue trace), (a) Cu-Phen, (b) Cu-DPQ-Phen, (c) Cu-DPPZ-Phen, and (d) Cu-DPPN-Phen. Electrochemical parameters (V) for complexes, and in the presence of added Na-L-ascorbate, and H_2O_2 (bottom). Analysis conducted in 10% v/v DMF; (i) complex without exogenous treatment (V), (ii) complex with added Na-L-ascorbate (V), and (iii) complex with added H_2O_2 (V).

reagents, $[Cu(DPQ)(Phen)]^{2+}$ and $[Cu(Phen)_2]^{2+}$, ablating H_2O_2 fluorescence at twice the rate of the DPPZ and DPPN complexes. Furthermore, given the series significant SODm activity and redox electrochemical profiles, it seems the rate-limiting factor in the chemical nuclease activity is, predominately, due to the subsequent metallo-hydroperoxo reaction.

DISCUSSION

The incorporation of designer phenazine ligands in the "bis-phen" $[Cu(Phen)_2]^{2+}$ chemical nuclease model pronounces DNA recognition and intercalation with significant enhancement to the dynamic binding constant for dipyrido[3,2-*f*:2′,3′-*h*]quinoxaline (DPQ) and dipyrido[3,2-*a*:2′,3′-*c*]phenazine (DPPZ) containing complexes; $[Cu(DPQ)(Phen)]^{2+}$ and $[Cu(DPPZ)(Phen)]^{2+}$. To our knowledge these binding constants ($K_{app} \approx 3 \times 10^7$ M(bp)$^{-1}$) are the highest reported to date for any existing copper(II) phenanthrene complex and surpass the $[Cu(Phen)_2]^{2+}$ cation by ∼60-fold. Additionally, these values compare favorably with the binding constants of Actinomycin D, identified in this study as 2.92×10^7 M(bp)$^{-1}$, and rhodium(III) complexes *rac*-$[Rh(phi)(phen)_2]^{3+}$ and *rac*-$[Rh(phi)_2(bipy)]^{3+}$ ($K_b \approx 10^6$–10^7 M^{-1})[35] (where phi = 9,10-phenanthrene-quinone-diimine and bpy = 2,2′-bipyridine) but do not match the ctDNA binding affinity of ruthenium(II) DPPZ complexes Δ-$[Ru(DPPZ)(Phen)_2]^{2+}$ or Λ-$[Ru(DPPZ)(Phen)_2]^{2+}$ ($K_{eff} \approx 10^8$ M^{-1}).[6] Indeed, the lowest binding constant among the three phenazine complexes generated ($K_{app} \approx 6 \times 10^6$ M(bp)$^{-1}$), observed for the $[Cu(DPPN)(Phen)]^{2+}$ complex, is on par with many high-affinity copper(II) binding constants in the literature.[36] Interestingly, copper(II) DPQ and DPPZ compounds have shown only mediocre DNA binding constants ($K_b = 10^4$–10^3 M^{-1}) when complexed with amino acid chelators L-leucine, L-tryptophan, and L-tyrosine which, surprisingly, have far lower binding constants than the amino acid complex $[Cu(glycine)(DPPZ)]^+$ ($K_b \approx 10^6$ M^{-1}), along with $[Cu(L\text{-arginine})(DPQ)]^+$ and $[Cu(L\text{-arginine})(DPPZ)]$ ($K_b \approx 10^5$ M^{-1} and $K_{app} \approx 10^6$ M^{-1}).[37−41] Enhanced binding constants ($K_{app} \approx 5 \times 10^6$ M^{-1}) were observed, however, for binuclear complexes $[\{Cu(DPQ)(DMF)\}_2(\mu\text{-OH})_2]^{2+}$ (DMF = dimethylformamide) and $[\{Cu(DPPZ)(DMF)\}_2(\mu\text{-OH})_2]^{2+}$, which feature two phenazine ligands spanning opposite directions along the hydroxide-bridged Cu−Cu axis.[42] Thus, in addition to the influence of an extended phenazine π-framework, our results suggest a prominent role for the ancillary chelated phenanthroline in nucleotide binding affinity. These ligands are presumably involved in secondary interactions with DNA bases or at the surface of the minor groove and may function to optimize complex binding geometry.[17,18,43]

The complex series has distinctive nucleotide binding specificity compared with netropsin and Actinomycin D. Their ability to similarly quench Hoechst 33258 and ethidium bromide-bound ctDNA fluorogenic dyes, along with their broadly analogous displacement of limited bound ethidium to poly[d(G-C)$_2$] and poly[d(A-T)$_2$], departs substantially from the observed binding specificity of these classical minor-groove binding or intercalating agents. Thermal melting analysis, however, reveals that both DPQ and DPPZ complexes extensively stabilize poly[d(G-C)$_2$] denaturation, comparable to Actinomycin D, and that the overall complex series has a large degree of similarity with this intercalator given their negligible stabilization on poly[d(A-T)$_2$]. Taken together, it appears likely that the complexes intercalate DNA at both the minor and major grooves, and these interactions are appreciably enhanced by the presence of coordinated phenazine ligands, in particular DPQ and DPPZ.

We reported a novel on-chip microfluidic method for the Agilent Bioanalyzer 2100 for examining, with high precision, chemical nuclease activity. In our view, this technique offers advantages over existing methodologies (e.g., band densitometry) in the quantitation of dsDNA damage and undoubtedly has application in quantifying the activity of cytotoxic DNA-damaging drugs, in particular those from families of structurally related agents. Further, this technique is suited for detecting sequence-specific metallodrug DNA interactions as in our laboratory we have observed the effects of introducing a second endonuclease (*sal*I) with single site-recognition specificity on this sequence. The analysis methods we have employed on the Bioanalyzer 2100 to detect DNA degradation involve both peak height and peak area intensity reduction. Our motivation for

dx.doi.org/10.1021/ic500914j | Inorg. Chem. 2014, 53, 5392−5404

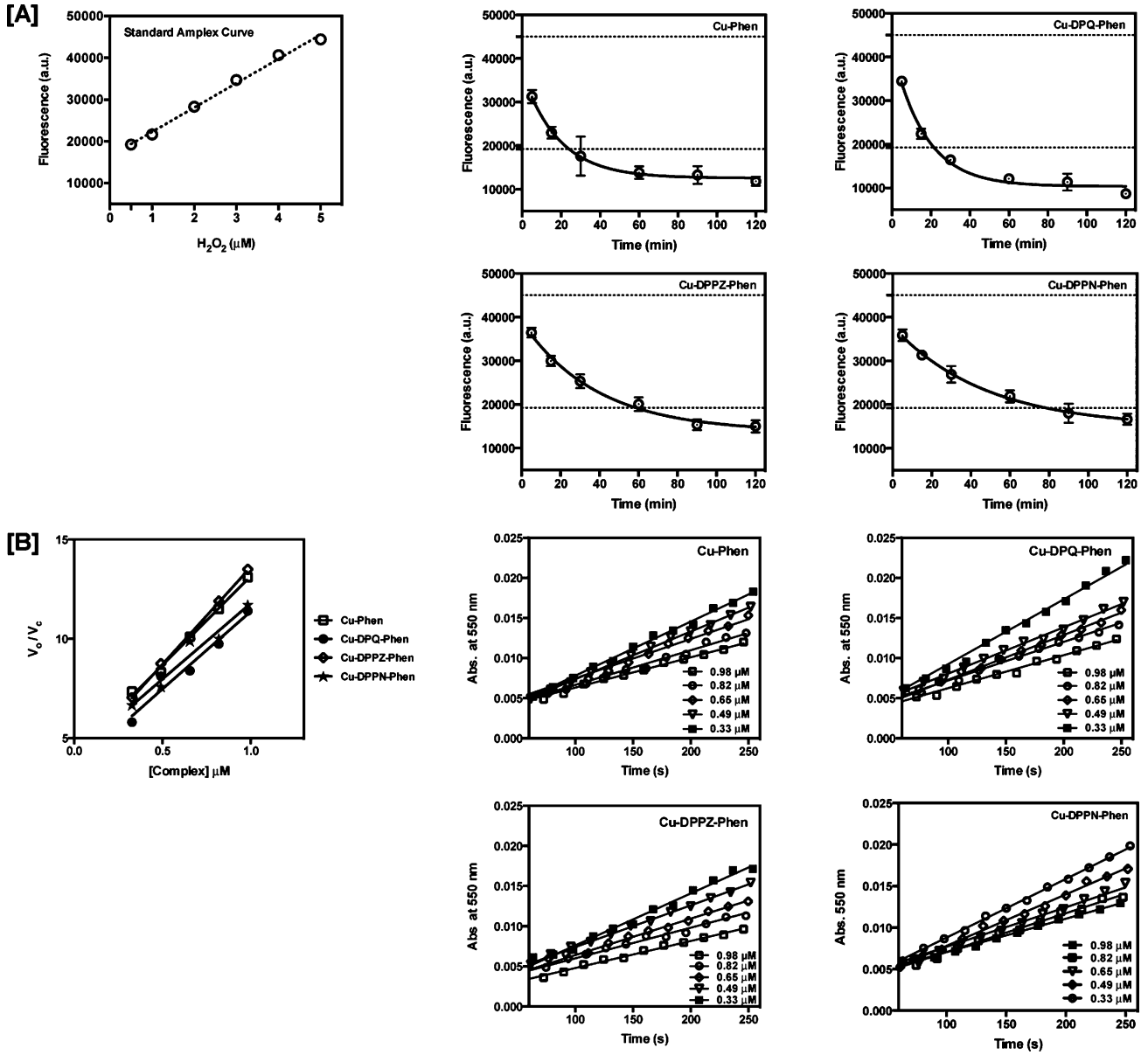

Figure 10. (A) Fenton-like degradation of hydrogen peroxide (5 μM) in the presence of metal complex (5 μM) and 100 μM Na-L-ascorbate, determined using the Amplex Red hydrogen peroxide assay kit (Invitrogen) (replicate experiments conducted on four separate occasions). A calibration curve is also shown, which details the linear ($r^2 > 0.99$) fluorescent response achieved from hydrogen peroxide detection in the assay. (B) Superoxide dismutase mimetic activity determined by the xanthine/xanthine oxidase system; metal complexes were examined between 0.98 and 0.33 μM at 25 °C under constant enzymatic production of superoxide (~1 μM/min) using the detector molecule nitro blue tetrazolium chloride, and this data was plotted as a function of catalytic rate in the absence/presence of catalyst (V_0/V_c) as a function of [complex] to yield the catalytic rate K_{cat} in units, M^{-1} s^{-1}.

applying both techniques stems from the observation that the Cu^{2+} complexes induced random damage, and thus asymmetric peak tailing on the pUC19 fragments (due to shearing chemical nuclease effects) were evident in each electrogram. This factor had an influence on peak area intensity, and so we found that peak height analysis was suitable to employ as a tandem method to enhance the overall accuracy of the technique. Our work revealed the $[Cu(DPQ)(Phen)]^{2+}$ complex as the most active chemical nuclease within this series; however, the degradation kinetics of this reagent is closely followed by $[Cu(Phen)_2]^{2+}$. The interaction of the phenazine complexes with pBC4 (59% G-C) and pUC19 (51% G-C) plasmid DNA, however, reveal significant differences compared with the $[Cu(Phen)_2]^{2+}$ cation in terms of chemical nuclease efficacy. $[Cu(Phen)_2]^{2+}$ had enhanced activity toward the lower G-C-containing plasmid (pUC19), while each of the phenazine complexes maintained, or enhanced, their activity toward the higher G-C-content plasmid (pBC4). These data suggest Cu^{2+} phenazine compounds may have targeting properties toward cytosine-phosphate-guanine (CpG) islands, which are found in the promoter regions of many mammalian genes.[44,45] Thus, it is of significant future importance to examine the DNA-targeting properties of these phenazine complexes within cisplatin-resistant cancer cell models such as SKOV3. While these complexes, in particular **Cu-DPPZ-Phen**, display interesting *in vitro* chemotherapeutic potential compared with doxorubicin on SKOV3, their targeted DNA-damaging effects have yet to be identified. Indeed, we recently reported that, although **Cu-Phen**

dx.doi.org/10.1021/ic500914j | Inorg. Chem. 2014, 53, 5392−5404

Table 4. Kinetic Properties of the Complex Series[a]

compound	H_2O_2 (Fenton) K (s^{-1})[b]	SODm K_{cat} (M^{-1} s^{-1})[c]
Cu-Phen	3.22	8.97×10^6
Cu-DPQ-Phen	3.54	7.82×10^6
Cu-DPPZ-Phen	1.56	9.80×10^6
Cu-DPPN-Phen	1.26	7.64×10^6

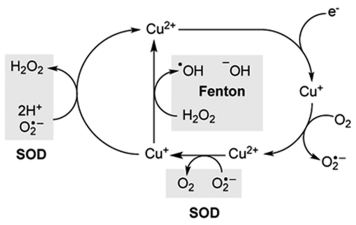

[a]Under Fenton-like and SODm conditions and catalytic cycle of Cu^+/Cu^{2+} ions with molecular oxygen, superoxide, and hydrogen peroxide. [b]Fenton degradation of 5 μM hydrogen peroxide in the presence of 5 μM complex and 100 μM Na-L-ascorbate. [c]Superoxide dismutase mimetic (SODm) activity determined by the xanthine/xanthine oxidase system.

has significant cytotoxic properties toward SKOV3, this agent nonselectively induces DNA damage and can be classified as a "promiscuous" cytotoxin.[27]

All complexes in this study have excellent superoxide dismutase mimetic activities (K_{cat} 7.6–9.8 $\times$ 10^6 M^{-1} s^{-1}) but are slow, kinetically, within the Fenton reaction ($Cu^+ + H_2O_2 \rightarrow Cu^{2+} + {}^{\bullet}OH + OH^-$). Significantly, however, Fenton breakdown follows linearized pUC19 chemical nuclease efficiency in the overall series (**Cu-DPQ-Phen** > **Cu-Phen** ≫ **Cu-DPPZ-Phen** > **Cu-DPPN-Phen**) with DPQ and the bis-phen complex consuming peroxide at twice the rate constant of DPPZ and DPPN reagents.

In summary, we showed that phenazine-functionalized Cu^{2+} phenanthroline complexes offer a clear enhancement toward DNA binding affinity relative to the well-studied $[Cu(Phen)_2]^{2+}$ cation and possess the highest ctDNA binding affinities currently known for Cu^{2+} phenanthrene complexes. We reported a new on-chip methodology for determining dsDNA degradation, and it is our opinion that both this technique and these Cu^{2+} phenazine reagents will have an important future role to play in the development of site-directed, gene-silencing, artificial metallonucleases for use as targeted chemotherapeutics for human disease.

MATERIALS AND METHODS

Preparation of Ligands and Metal Complexes. Chemicals and reagents of analytical grade for the preparation of organic ligands and metal complexes were purchased from Sigma-Aldrich (Ireland) and used without further purification.

Preparation of 1,10-Phenanthroline-5,6-dione (Phendio). Phendio was prepared according to the literature method reported by Dickeson and Summers, with slight modification.[24] 1,10-Phenanthroline (4.00 g, 22.19 mmol) and potassium bromide (4.00 g, 33.6 mmol) were thoroughly mixed and slowly added to an ice-cold mixture of H_2SO_4 (40 mL) and HNO_3 (20 mL). The solution was refluxed for 3 h at 100 °C, then cooled to room temperature, poured onto crushed ice (~400 mL), and neutralized with an aqueous NaOH solution (80.0 g per 400 mL) to a pH between 4 and 5, yielding a yellow solution. The solution was extracted with $CHCl_3$ (in 8 $\times$ 100 mL portions). The organic phase was combined and dried with anhydrous magnesium sulfate and then filtered before being evaporated to dryness, whereupon a bright yellow solid (4.03 g) was obtained. The product could be further purified by recrystallization from high-performance liquid chromatography (HPLC)-grade methanol but was sufficiently pure to use in subsequent reactions. Yield: 4.03 g (86%). ^{1}H NMR (400 MHz, $CDCl_3$): 9.05 (dd, J = 4.6, 1.8 Hz, 2H), 8.44 (dd, J = 7.9, 1.8 Hz, 2H), 7.52 (dd, J = 7.9, 4.6 Hz, 2H). IR (ATR, cm^{-1}): 3348, 3061, 1678, 1559, 1458, 1412, 1290, 1204, 1114, 1009, 924, 806, 734. Solubility: DMF, EtOH, DMSO (partially), melting point (mp) 258–260 °C.

Preparation of Dipyrido[3,2-*f*:2′,3′-*h*]quinoxaline (DPQ). DPQ was prepared according to the literature method reported by Hambley et al., with some modification.[26] To a solution of phendio (0.510 g, 2.44 mmol) in water (35 mL) was added ethylenediamine (0.70 mL, 10.47 mmol), and the resultant suspension was refluxed for 12 h at 60 °C. The resulting product was washed with water (10 mL) and minimum volume of diethyl ether. Yield: 0.372 g (66%). ^{1}H NMR (400 MHz, $CDCl_3$): 9.47 (dd, J = 8.2, 1.8 Hz, 2H), 9.24 (dd, J = 4.3, 1.8 Hz, 2H), 9.19 (s, 2H), 7.96 (dd, J = 8.2, 4.3 Hz, 2H). IR (ATR, cm^{-1}): 2990, 1570, 1472, 1466, 1206, 1073, 1077, 825, 803, 739. Solubility: DMF, EtOH, DMSO (partially). mp 330–335 °C.

Preparation of Dipyrido[3,2-*a*:2′,3′-*c*]phenazine (DPPZ). DPPZ was prepared according to literature, with slight changes made to the method.[24] A methanolic solution (20 mL) of 1,2-phenylenediamine dihydrochloride (0.640 g, 3.53 mmol) was refluxed until it was dissolved. A warm ethanolic solution of phendio (0.500 g, 2.38 mmol) was prepared (20 mL), added over the methanolic solution, and refluxed with constant stirring for 3 h. The resulting solution was vacuum-filtered and recrystallized from EtOH, producing metallic-like orange filaments. Yield: 0.521 g (78%). ^{1}H NMR (400 MHz, $CDCl_3$): 9.58 (dd, J = 8.1, 1.7 Hz, 2H), 9.20 (dd, J = 4.5, 1.7 Hz, 2H), 8.29 (dd, J = 6.5, 3.4 Hz, 2H), 7.86 (dd, J = 6.5, 3.4 Hz, 2H), 7.73 (dd, J = 8.1, 4.5 Hz, 2H). IR (ATR, cm^{-1}): 3040, 1615, 1570, 1486, 1412, 1336, 1077, 1072, 808, 739. Solubility: DMF, EtOH, DMSO (partially). mp 248–253 °C.

Preparation of Benzo[*l*]dipyrido[3,2-*a*:2′,3′-*c*]phenazine (DPPN). DPPN was prepared according to literature, with slight changes made to the method.[25] To a solution of phendio (0.300 g, 1.422 mmol) in EtOH (45 mL) was added 2,3-diaminonaphthalene (0.339 g, 2.136 mmol), and the resulting suspension was refluxed for 3 h, during which time an orange precipitate formed. The precipitate was vacuum-filtered, washed with cold ethanol, and allowed to dry. Yield: 0.443 g (93%). ^{1}H NMR (400 MHz, $CDCl_3$): 9.49 (dd, J = 8.1, 1.8 Hz, 2H), 9.16 (dd, J = 4.4, 1.8 Hz, 2H), 8.80 (s, 2H), 8.09 (dd, J = 6.5, 3.1 Hz, 2H), 7.68 (dd, J = 8.1, 4.4 Hz, 2H), 7.53 (dd, J = 6.5, 3.1 Hz, 2H). IR (ATR, cm^{-1}): 3362, 1628, 1583, 1565, 1409, 1360, 1274, 1128, 1070, 1033, 892, 871, 850, 817. Solubility: DMF (partially). mp 283–285 °C.

Preparation of [Cu(Phen)](NO$_3$)$_2$. To a solution of copper(II) nitrate hemipentahydrate (1 g, 4.3 mmol) in EtOH (75 mL) was added Phen (0.78 g, 4.3 mmol), and the resulting suspension was refluxed for 2 h. The solution was left to stand for 12 h, vacuum-filtered, and washed with a minimum volume of cold EtOH. Yield: 1.43 g (90%). Anal. Calc. for $C_{12}H_8CuN_4O_6$: C, 39.19; H, 2.19; N, 15.23. %Found: C, 39.65; H, 2.06; N, 14.92. IR (ATR, cm^{-1}): 3068, 1583, 1451, 1426, 1270, 1151, 1110, 1011, 972, 847, 807, 739, 719. Solubility: DMF, EtOH.

Preparation of [Cu(Phen)$_2$](NO$_3$)$_2$ (Cu-Phen). This complex was prepared according to the method reported by Prisecaru et al.[27]

dx.doi.org/10.1021/ic500914j | Inorg. Chem. 2014, 53, 5392–5404

General Procedure for Preparing [Cu(*N*,*Ń*)(Phen)]$(NO_3)_2$ Complexes (where *N*,*Ń* = DPPZ, DPPN, and DPQ). To a solution of [Cu(phen)$(NO_3)_2$] (0.1 g, 0.27 mmol) in EtOH (30 mL) was added 0.27 mmol of either DPQ (0.063 g), DPPZ (0.076 g), or DPPN (0.090 g), and the resulting suspension was stirred for 12 h at 50 °C. The solution was vacuum-filtered and washed with a minimum volume of cold EtOH.

[Cu(DPQ)(Phen)]$(NO_3)_2$·0.5H_2O (Cu-DPQ-Phen). Yield: 0.1207 g (73%). Anal. Calc. for $C_{26}H_{17}CuN_8O_{6.5}$: C, 51.28; H, 2.81; N, 18.40. %Found: C, 51.15; H, 2.29; N, 18.68. IR (ATR, cm^{-1}): 3034, 1581, 1472, 1360, 1288, 1210, 1081, 818, 718. Solubility: EtOH, MeOH, DMF, DMSO (partially).

[Cu(DPPZ)(Phen)]$(NO_3)_2$ (Cu-DPPZ-Phen). Yield: 0.0709 g (41%). Anal. Calc. for $C_{30}H_{18}CuN_8O_6$: C, 55.43; H, 2.79; N, 17.24. %Found: C, 56.38; H, 2.88; N, 17.83. IR (ATR, cm^{-1}): 3023, 1578, 1451, 1376, 1292, 1076, 819, 718, 729. Solubility: DMF, DMSO (partially).

[Cu(DPPN)(Phen)]$(NO_3)_2$·2H_2O (Cu-DPPN-Phen). Yield: 0.1341 g (67%). Anal. Calc. for $C_{34}H_{24}CuN_8O_8$: C, 55.47; H, 3.29; N, 15.22. %Found: C, 55.42; H, 2.76; N, 15.38. IR (ATR, cm^{-1}): 3020, 1578, 1518, 1375, 1358, 1290, 1046, 868, 719. Solubility: DMF, DMSO (partially).

DNA Binding Studies. The fluorescence-quenching assay, the competitive ethidium bromide displacement assay, and the viscosity measurements we all conducted according to the method reported by Kellett et al.[28]

Fluorescence Quenching for poly[d(A-T)$_2$] and poly[d(G-C)$_2$]. Solutions of double-stranded alternating copolymers poly[d(A-T)·d(A-T)] (Sigma PO883, ε_{260} = 13 100 M $(bp)^{-1}$ cm^{-1}) and poly[d(G-C)·d(G-C)] (Sigma P9389, ε_{260} = 16 800 $M(bp)^{-1}$ cm^{-1}) were prepared in nuclease-free water and quantified on a Cary 100 UV–visible spectrophotometer. A working solution of 50 μM poly[d(A-T)$_2$] (or poly[d(G-C)$_2$]) along with 10 μM ethidium bromide (EtBr) in *N*-(2-hydroxyethyl)piperazine-*N*′-ethanesulfonic acid (HEPES) buffer (80 mM, pH = 7.2) and NaCl (40 mM) was prepared. Stock solutions of metal complexes, metal salts, and groove-binding drugs were prepared at ∼4 mM in DMF and were further diluted to 80 mM in HEPES buffer. 50 μL of the poly[d(A-T)$_2$] (or (poly[d(G-C)$_2$]) EtBr working solution was placed in each well of a 96-well microplate with the exception of the blanks, which contained 95 μL of 80 mM HEPES and 5 μM EtBr. Serial aliquots of the tested compound were added to the working solutions, and the volume was adjusted to 100 μL in each well such that the final concentrations of nucleotide and EtBr were 25 μM and 5 μM, respectively. The plate was then allowed to incubate at room temperature for 5 min before being analyzed using a Bio-Tek synergy HT multimode microplate reader with excitation and emission wavelengths being set to 530 and 590 nm for EtBr detection. Concentrations of the tested compounds were optimized such that fluorescence was 30–40% of the initial control at their highest reading. Each drug concentration was measured in duplicate. From a plot of fluorescence versus added drug concentration, the *Q* value is given by the concentration required to effect 50% removal of the initial fluorescence of the bound dye.

Thermal Melting Experiments. Analysis was carried out on an Agilent Cary 100 dual beam spectrophotometer equipped with a 6 × 6 Peltier multicell system with temperature controller. For poly[d(G-C)$_2$]; in a final volume of 1 mL using Starna black-walled quartz cuvettes with tight-fitting seals, 2 mM NaOAc buffer (pH = 5.0), 1 mM NaCl and poly[d(G-C)$_2$] (Sigma, P9389) were added to give a final absorbance of between 0.18 and 0.20 absorbance units at 260 nm (ε_{max} = 8400 M^{-1} cm^{-1}). For poly[d(A-T)$_2$]; in a final volume of 1 mL using Starna black-walled quartz cuvettes with tight-fitting seals, 50 mM NaOAc buffer (pH = 5.0), 250 mM NaCl and poly[d(A-T)$_2$] (Sigma, PO883) were added to give a final absorbance of between 0.18 and 0.20 absorbance units at 260 nm (ε_{max} = 6600 M^{-1} cm^{-1}). Stock solutions of metal complexes, netropsin, and Actinomycin D, prepared beforehand in DMF, were dissolved in 80 mM HEPES (pH 7.2). An aliquot of test reagent was then added to each cuvette such that an *r* value of 0.1 was achieved (*r* = [compound]/[nucleotide]). The test reagent and respective alternating copolymer were then incubated for 10 min at 20 °C prior to commencing the temperature ramp. Thermal melting measurements were recorded at 260 nm at 0.25 s intervals. Temperature was ramped at 3 °C/min over the range of 20.0–97.0 °C. The spectral bandwidth (SBW) was set to 1. Temperature was calibrated, for each measurement, using a temperature probe placed in an identical black-walled cuvette containing equivalent buffer and NaCl. Samples were run in triplicate, and the melting temperature T_M (°C) was calculated using the built-in derivative method on the instrument.

Artificial Metallonuclease Activity. **Generation of pUC19 DNA.** The vector pUC19 was generated following the transformation of *E. coli* using an LB ampicillin-resistant media protocol, extracted using a maxi-prep kit protocol (NucleoBond Xtra Midi Plus, EF-Macherey-Nagel), and then quantified using the NanoDrop (ND-1000 Spectrophotometer).

Gel Electrophoresis Experiments on pUC19 DNA. Reactions were carried out according to the literature procedure by Kellett et al.[46] Briefly, in a total volume of 20 μL using 80 *m*M HEPES buffer (Fisher) at pH 7.2 with 25 mM NaCl, an aliquot of the stock complex (prepared in DMF) was mixed with 400 ng of supercoiled pUC19 and 1 μL of 20 mM Na-L-ascorbate. Samples were incubated for 30 min at 37 °C before being quenched with 6X loading dye (Fermentas), containing 10 mM tris(hydroxymethyl)aminomethane-HCl (pH 7.6), 0.03% bromophenol blue, 0.03% xylene cyanol, 60% glycerol, and 60 mM EDTA, then loaded onto agarose gel (1%) containing 2.0 μL of GelRed (10 000X). Electrophoresis was completed at 80 V for 1.5 h using a wide mini-sub cell (BioRad) in 1X Tris–acetate–EDTA buffer (Millipore). Trapping experiments with 100 μM neocuprione (Sigma, N1501), 10% v/v DMSO, 1000 units of bovine SOD enzyme (Sigma, S7571), and 1000 units of catalase enzyme from bovine liver (Sigma, C1345) were also examined using this procedure.

Linearization of Supercoiled pUC19. In a total volume of 20 μL, using 5 μg of supercoiled pUC19, 5 μL of 10X HEPES buffer, 2.5 μL of 20 000 U/mL *Hin*dIII (NEB), 5 μL of NEBuffer 2 (NEB), 1 μL of bovine serum albumin (BSA) (NEB) and nuclease-free water were added. This mixture was allowed to incubate at 37 °C for 2.5 h, after which 1 μL of this mixture was loaded onto an agarose gel to confirm linearization. Linear DNA from the mixture was then purified from the enzymatic reaction, using a QIAquick Purification column (QIAGEN). Linearized DNA was quantified using the NanoDrop (ND-1000 Spectrophotometer).

Microfluidic Chip Analysis of DNA Degradation on the Agilent Bioanalyzer 2100. In a total volume of 20 μL, using 80 mM HEPES buffer (Fisher) at pH 7.2 with 25 mM NaCl, the complex (500 nM) was mixed with 400 ng of linear pUC19 and 1 mM Na-L-ascorbate. Samples were incubated at 37 °C for between 1 and 30 min and quenched with both neocuproine (100 μM) and EDTA (100 μM) before being loaded onto a DNA 7500 microfluidic chip as per the manufacturer's protocol.[23] Data was then collected using Agilent 2100 Bioanalyzer. Electrograms generated by the Bioanalyzer 2100 for all complexes are available in the Supporting Information.

Chemical Nuclease of Linearized pUC19. In a total volume of 20 μL, using 400 ng of supercoiled pUC19 (2686 bp), 1 μL of *Sal*I (20 000 U/mL, NEB, cleaving the plasmid at one site located at 429 bp), 2 μL of 10X HEPES buffer, 2 μL of NEBuffer 3.1, and nuclease-free water were added. The reaction mixture was allowed to incubate at 37 °C for 1.5 h, after which the endonuclease was heat-inactivated at 65 °C for 20 min. After the mixture was cooled, an aliquot of the stock complex and 1 mM Na-L-ascorbate were added to the reaction mixture, and the final concentration of EDTA was adjusted (where appropriate) to ensure a final concentration 40.0 μM before incubation at 37 °C for 30 min was completed. The reaction was then quenched with 6X loading dye (Fermentas), and DNA fragments were subjected to gel electrophoresis (prepared and stained as previously described).

Chemical Nuclease of Linearized pBC4. In a total volume of 20 μL, using 400 ng of supercoiled pBC4 (10 673 bp), 1 μL of *Age*I (20 000 U/mL, NEB, cleaving the plasmid at one site located at 5037 bp), 2 μL of 10X HEPES buffer, 2 μL of NEBuffer 1, 0.2 μL of BSA and nuclease-free water were added. Reaction mixture was allowed to incubate at 37 °C for 1.5 h, after which the endonuclease was heat-

dx.doi.org/10.1021/ic500914j | *Inorg. Chem.* 2014, 53, 5392–5404

inactivated at 65 °C for 20 min. After the mixture was cooled, an aliquot of the stock complex and 1 mM Na-L-ascorbate were added to the reaction mixture, and the final concentration of EDTA was adjusted (where appropriate) to ensure a final concentration 40.0 μM before incubation at 37 °C for 30 min was completed. The reaction was then quenched with 6X loading dye (Fermentas), and DNA fragments were subjected to gel electrophoresis (prepared and stained as previously described).

Cell Culture Experiments. SKOV-3 cells were grown in RPMI 1640 supplemented with 10% fetal calf serum (FCS) at 37 °C in a humidified atmosphere with 5% CO_2. Compound viability was tested using Guava Viacount (Millipore) reagent following 24 h exposure. Positive control, doxorubicin, was purchased from Sigma-Aldrich as a European Pharmacopoeia reference standard. DMSO stocks for the complexes **Cu-Phen**, **Cu-DPQ-Phen**, **Cu-DPPZ-Phen**, **Cu-DPPN-Phen**, and doxorubicin were prepared in 1 mL, ranging from 11 to 34 mM.

ViaCount Assay. SKOV3 cells were seeded at an initial density of 4×10^4 cell/mL in 96-well plates and incubated overnight prior to drug addition. DMSO stocks of the complexes and controls were diluted in RPMI 1640 containing 10% FCS, to give the following final concentrations in 200 μL wells: 5.0, 2.5, 1.0, 0.5, and 0.25 μM. A DMSO control of the highest incubation concentration was also included. Cells were incubated for 24 h at 37 °C in a humidified atmosphere with 5% CO_2. After 24 h of exposure, spent media was removed, and cells were washed once with 200 μL of phosphate-buffered saline and detached using 50 μL of 1X trypsin, with the subsequent addition of 50 μL of media. Cells were transferred to 96-well round-bottom plates with 100 μL of ViaCount reagent incubated at room temperature in the dark for 10 min. Viability data was collected on Guava EasyCyte HT flow cytometer using Guava Viacount software.

Electrochemistry. Electrochemical measurements were performed on a Solartron 1825 potentiostat, and data were analyzed using *CorrView* software. Electrochemistry was performed in 1 mM solutions of each complex, made up in 0.1 M tetrabutylammonium hexafluorophosphate ($TBAPF_6$) in 10% v/v DMF as the supporting electrolyte. Concentrations of added reductant and oxidant were 2 mM to ensure an excess was present in solution (ratio 1:2, complex/(reductant/oxidant)). Electrochemical cell setup: Glassy Carbon working electrode (2 mm diameter), platinum wire counter electrode, nonaqueous Ag/Ag^+ reference electrode ($E_{1/2}$ = 0.075 V versus Fc/Fc^+). Glassy carbon electrodes were polished using alumina oxide powder (0.05 μm) on a microcloth (Buehler). Cyclic voltammetric data presented were obtained after steady-state was attained, at a scan rate of 100 mV s^{-1}, with scans initiating in the cathodic direction.

Superoxide Dismutase Mimetic Activity. The SOD mimetic activities of the complexes were determined using a nitro blue tetrazolium (NBT) assay,[34] in which the xanthine/xanthine oxidase system serves as the source of superoxide radicals. The quantitative reduction of NBT to blue formazan by $O_2^{\bullet-}$ was followed spectrophotometrically using a thermostatically controlled Agilent Cary 100 dual-beam spectrophotometer at 550 nm at 25 °C. Reagents were obtained from Sigma–Aldrich, and the assays were run in a total volume of 3 mL. Tabulated results were derived from linear regression analyses and are reported as rate in the absence of catalyst/rate in the presence (V_o/V_c) versus catalyst concentration, which yielded the catalytic rate (K_{cat} M^{-1} s^{-1}).

H_2O_2 Breakdown Assay. A 5 mL stock solution of 100 μM Amplex Red containing 10 mM Amplex Red reagent and 10 U/ml horseradish peroxidase (HRP) was prepared in 1X buffer as per Amplex Red hydrogen Peroxide/Peroxidase assay kit instruction (Invitrogen—Cat. A22188). A standard fluorescence response curve from H_2O_2 was obtained by adding a series of aliquots (0.5–5 μM) of H_2O_2 and the Amplex Red stock solution, and the volume was adjusted to 100 μL with 1X buffer in each sample well. An aliquot containing 5 μM of tested compounds, 5 μM H_2O_2, and 100 μM Na-L-ascorbate that were previously incubated between 0–120 min was added to 50 μL of Amplex Red solution, and again the volume was adjusted to 100 μL using 1X buffer. The fluorescence intensity of the reaction mixture was measured with a Bio-Tek synergy HT multimode microplate reader equipped with excitation and emission filters at 530 and 590 nm.[47]

■ ASSOCIATED CONTENT

Ⓢ Supporting Information

Electrogram and electropherogram data from the Bioanalyzer 2100, optimization experiments for polynucleotide thermal melting, and nonlinear regression curves for cytotoxicity toward SKOV3 cells. This material is available free of charge via the Internet at http://pubs.acs.org.

■ AUTHOR INFORMATION

Corresponding Author

*Email: andrew.kellett@dcu.ie. Phone: +353 (0)1 7005461.

Author Contributions

Authors Zara Molphy and Andreea Prisecaru contributed equally to this work.

Notes

The authors declare no competing financial interest.

■ ACKNOWLEDGMENTS

This work was supported by the Dublin City University Career Start fund, Irish Research Council (IRC) grants, GOIPG/2013/826 and GOIPG/2013/937, Dublin City University Distinguished Scholars Studentship award and EU COST Action CM1201: Biomimetic Radical Chemistry.

■ REFERENCES

(1) Liu, H.-K.; Sadler, P. J. *Acc. Chem. Res.* **2011**, *44*, 349.
(2) Jamieson, E. R.; Lippard, S. J. *Chem. Rev.* **1999**, *99*, 2467.
(3) Lippard, S.; Bond, P.; WU, K.; Bauer, W. *Science* **1976**, *194*, 726.
(4) Zeglis, B. M.; Pierre, V. C.; Barton, J. K. *Chem. Commun.* **2007**, 4565.
(5) Park, G. Y.; Wilson, J. J.; Song, Y.; Lippard, S. J. *Proc. Natl. Acad. Sci. U.S.A.* **2012**, *109*, 11987.
(6) Hiort, C.; Lincoln, P.; Norden, B. *J. Am. Chem. Soc.* **1993**, *115*, 3448.
(7) Sigman, D. S.; Graham, D. R.; D'Aurora, V.; Stern, A. M. *J. Biol. Chem.* **1979**, *254*, 12269.
(8) Sigman, D. S.; Mazumder, A.; Perrin, D. M. *Chem. Rev.* **1993**, *93*, 2295.
(9) Chen, C.-h. B.; Milne, L.; Landgraf, R.; Perrin, D. M.; Sigman, D. S. *ChemBioChem.* **2001**, *2*, 735.
(10) Santini, C.; Pellei, M.; Gandin, V.; Porchia, M.; Tisato, F.; Marzano, C. *Chem. Rev.* **2013**.
(11) Gutteridge, J. M. C.; Halliwell, B. *Biochem. Pharmacol.* **1982**, *31*, 2801.
(12) Goldstein, S.; Michel, C.; Bors, W.; Saran, M.; Czapski, G. *Free Radical Biol. Med.* **1988**, *4*, 295.
(13) Sigman, D. S.; Bruice, T. W.; Mazumder, A.; Sutton, C. L. *Acc. Chem. Res.* **1993**, *26*, 98.
(14) Chen, C. H.; Sigman, D. S. *Proc. Natl. Acad. Sci. U.S.A.* **1986**, *83*, 7147.
(15) Bales, B. C.; Kodama, T.; Weledji, Y. N.; Pitié, M.; Meunier, B.; Greenberg, M. M. *Nucleic Acids Res.* **2005**, *33*, 5371.
(16) Pitié, M.; Burrows, C. J.; Meunier, B. *Nucleic Acids Res.* **2000**, *28*, 4856.
(17) Niyazi, H.; Hall, J. P.; O'Sullivan, K.; Winter, G.; Sorensen, T.; Kelly, J. M.; Cardin, C. J. *Nat. Chem.* **2012**, *4*, 621.
(18) Song, H.; Kaiser, J. T.; Barton, J. K. *Nat. Chem.* **2012**, *4*, 615.
(19) Holmlin, R. E.; Dandliker, P. J.; Barton, J. K. *Angew. Chem., Int. Ed. Engl.* **1997**, *36*, 2714.
(20) Hall, J. P.; Cook, D.; Morte, S. R.; McIntyre, P.; Buchner, K.; Beer, H.; Cardin, D. J.; Brazier, J. A.; Winter, G.; Kelly, J. M.; Cardin, C. J. *J. Am. Chem. Soc.* **2013**, *135*, 12652.

(21) Wang, J. *Nucleic Acids Res.* **2000**, *28*, 3011.
(22) Agilent Technologies. http://www.agilent.com/ (accessed January, 2013).
(23) Agilent Technologies Genomics. http://www.genomics.agilent.com/en/Bioanalyzer-DNA-RNA-Kits/DNA-Analysis-Kits/?cid=AG-PT-105&tabId=AG-PR-1040 (accessed January, 2013).
(24) Dickeson, J.; Summers, L. *Aust. J. Chem.* **1970**, *23*, 1023.
(25) Yam, V. W.-W.; Lo, K. K.-W.; Cheung, K.-K.; Kong, R. Y.-C. *Chem. Commun.* **1995**, 1191.
(26) Collins, J. G.; Sleeman, A. D.; Aldrich-Wright, J. R.; Greguric, I.; Hambley, T. W. *Inorg. Chem.* **1998**, *37*, 3133.
(27) Prisecaru, A.; McKee, V.; Howe, O.; Rochford, G.; McCann, M.; Colleran, J.; Pour, M.; Barron, N.; Gathergood, N.; Kellett, A. *J. Med. Chem.* **2013**, *56*, 8599.
(28) McCann, M.; McGinley, J.; Ni, K.; O'Connor, M.; Kavanagh, K.; McKee, V.; Colleran, J.; Devereux, M.; Gathergood, N.; Barron, N.; Prisecaru, A.; Kellett, A. *Chem. Commun.* **2013**, *49*, 2341.
(29) O'Connor, P. M.; Jackman, J.; Bae, I.; Myers, T. G.; Fan, S.; Mutoh, M.; Scudiero, D. A.; Monks, A.; Sausville, E. A.; Weinstein, J. N.; Friend, S.; Fornace, A. J., Jr.; Kohn, K. W. *Cancer Res.* **1997**, *57*, 4285.
(30) O'Neill, C. F.; Koberle, B.; Masters, J. R. W.; Kelland, L. R. *Br. J. Cancer.* **1999**, *81*, 1294.
(31) Momparler, R. L.; Karon, M.; Siegel, S. E.; Avila, F. *Cancer Res.* **1976**, *36*, 2891.
(32) Capranico, G.; Kohn, K. W.; Pommier, Y. *Nucleic Acids Res.* **1990**, *18*, 6611.
(33) Pang, B.; Qiao, X.; Janssen, L.; Velds, A.; Groothuis, T.; Kerkhoven, R.; Nieuwland, M.; Ovaa, H.; Rottenberg, S.; van Tellingen, O.; Janssen, J.; Huijgens, P.; Zwart, W.; Neefjes, J. *Nat. Commun.* **2013**, *4*, 1908.
(34) Goldstein, S.; Czapski, G. *Free Radicals: A Practical Approach;* IRL Press at Oxford University Press: New York, 1996.
(35) Arkin, M. R.; Stemp, E. D. A.; Turro, C.; Turro, N. J.; Barton, J. K. *J. Am. Chem. Soc.* **1996**, *118*, 2267.
(36) Liu, Z.-C.; Wang, B.-D.; Yang, Z.-Y.; Li, Y.; Qin, D.-D.; Li, T.-R. *Eur. J. Med. Chem.* **2009**, *44*, 4477.
(37) Chen, J.; Ren, X.; Le, X.; Feng, X. *Chin. J. Chem.* **2010**, *28*, 2179.
(38) Le, X. Y.; Gu, Q.; Song, Z. J.; Zhuang, C. X.; Feng, X. L. *J. Coord. Chem.* **2007**, *60*, 1359.
(39) Rao, R.; Patra, A. K.; Chetana, P. R. *Polyhedron* **2008**, *27*, 1343.
(40) Terenzi, A.; Tomasello, L.; Spinello, A.; Bruno, G.; Giordano, C.; Barone, G. *J. Inorg. Biochem.* **2012**, *117*, 103.
(41) Patra, A. K.; Bhowmick, T.; Roy, S.; Ramakumar, S.; Chakravarty, A. R. *Inorg. Chem.* **2009**, *48*, 2932.
(42) Thomas, A. M.; Nethaji, M.; Chakravarty, A. R. *J. Inorg. Biochem.* **2004**, *98*, 1087.
(43) Liu, J.-G.; Zhang, Q.-L.; Shi, X.-F.; Ji, L.-N. *Inorg. Chem.* **2001**, *40*, 5045.
(44) Jaenisch, R.; Bird, A. *Nat. Genet.* **2003**, *33*, 245.
(45) Spruijt, Cornelia G.; Gnerlich, F.; Smits, Arne H.; Pfaffeneder, T.; Jansen, Pascal W. T. C.; Bauer, C.; Münzel, M.; Wagner, M.; Müller, M.; Khan, F.; Eberl, H. C.; Mensinga, A.; Brinkman, Arie B.; Lephikov, K.; Müller, U.; Walter, J.; Boelens, R.; van Ingen, H.; Leonhardt, H.; Carell, T.; Vermeulen, M. *Cell* **2013**, *152*, 1146.
(46) Prisecaru, A.; Devereux, M.; Barron, N.; McCann, M.; Colleran, J.; Casey, A.; McKee, V.; Kellett, A. *Chem. Commun.* **2012**, *48*, 6906.
(47) Rhee, S.; Chang, T.-S.; Jeong, W.; Kang, D. *Mol. Cells* **2010**, *29*, 539.